Ultra-slim plastic endomicroscope objective for non-linear microscopy

Matthew Kyrish,[1] Urs Utzinger,[2,3] Michael R. Descour,[2] Brenda K. Baggett,[3] and Tomasz S. Tkaczyk[1,*]

[1]*Department of Bioengineering, Rice University, MS 142, 6100 Main St., Houston, Texas, 77005, USA*
[2]*College of Optical Sciences, University of Arizona, 1630 E. University Blvd., Tucson, Arizona, 85721, USA*
[3]*Biomedical Engineering, University of Arizona, 1657 E Helen Street, Tucson, Arizona 85721, USA*
**ttkaczyk@rice.edu*

Abstract: Non-linear microscopy has the potential to provide clinically useful information on the structure of biological tissue *in vivo* via an endomicroscope. The ability to use plastic as the optical material in a multiphoton objective was evaluated based on several criteria including autofluorescence, injection molding induced birefringence, and pulse broadening due to group velocity dispersion. An all-plastic, refractive ultra-slim endoscope objective was built with design specifications of NA = 0.4, FOV = 250 μm, 1.27 mm outer diameter, and 0.8 mm clear aperture. Initial images of second-harmonic generation signal (illumination at 780 nm) in collagen fibers and two-photon excited fluorescence (illumination at 920 nm) of *Convallaria* rhizome are reported.

OCIS codes: (350.3950) Micro-optics; (170.2150) Endoscopic imaging; (170.3880) Medical and biological imaging; (180.4315) Nonlinear microscopy.

References and links

1. S. Mukherjee, J. S. Wysock, C. K. Ng, M. Akhtar, S. Perner, M. M. Lee, M. A. Rubin, F. R. Maxfield, W. W. Webb, and D. S. Scherr, "Human bladder cancer diagnosis using multiphoton microscopy," in Photonic Therapeutics and Diagnostics V, N. Kollias, ed. (SPIE, 2009).
2. M. Göppert-Mayer, "Über Elementarakte mit zwei Quantensprüngen," Annalen der Physik **401**(3), 273–294 (1931).
3. W. Denk, J. H. Strickler, and W. W. Webb, "Two-photon laser scanning fluorescence microscopy," Science **248**(4951), 73–76 (1990).
4. P. Cheng and C. K. Sun, "Nonlinear (harmonic generation) optical microscopy," in Handbook of Confocal Microscopy, J. Pawley, ed., (Springer, 2006).
5. L. Gao, L. Jin, P. Xue, J. Xu, Y. Wang, H. Ma, and D. Chen, "Reconstruction of complementary images in second harmonic generation microscopy," Opt. Express **14**(11), 4727–4735 (2006).
6. R. M. Williams, W. R. Zipfel, and W. W. Webb, "Multiphoton microscopy in biological research," Curr. Opin. Chem. Biol. **5**(5), 603–608 (2001).
7. F. Helmchen, M. S. Fee, D. W. Tank, and W. Denk, "A miniature head-mounted two-photon microscope. high-resolution brain imaging in freely moving animals," Neuron **31**(6), 903–912 (2001).
8. D. Bird and M. Gu, "Two-photon fluorescence endoscopy with a micro-optic scanning head," Opt. Lett. **28**(17), 1552–1554 (2003).
9. L. Fu, A. Jain, H. Xie, C. Cranfield, and M. Gu, "Nonlinear optical endoscopy based on a double-clad photonic crystal fiber and a MEMS mirror," Opt. Express **14**(3), 1027–1032 (2006).
10. R. Le Harzic, M. Weinigel, I. Riemann, K. König, and B. Messerschmidt, "Nonlinear optical endoscope based on a compact two axes piezo scanner and a miniature objective lens," Opt. Express **16**(25), 20588–20596 (2008).
11. K. König, A. Ehlers, I. Riemann, S. Schenkl, R. Bückle, and M. Kaatz, "Clinical two-photon microendoscopy," Microsc. Res. Tech. **70**(5), 398–402 (2007).
12. S. Schenkl, A. Ehlers, R. LeHarzic, M. Stark, I. Riemann, B. Messerschmidt, M. Kaatz, and K. König, "Rigid and high NA multiphoton fluorescence GRIN-endoscopes," in Novel Optical Instrumentation for Biomedical Applications III, C. D. Depeursinge, ed. (SPIE, 2007).
13. J. N. Rogart, J. Nagata, C. S. Loeser, R. D. Roorda, H. Aslanian, M. E. Robert, W. R. Zipfel, and M. H. Nathanson, "Multiphoton imaging can be used for microscopic examination of intact human gastrointestinal mucosa ex vivo," Clin. Gastroenterol. Hepatol. **6**(1), 95–101 (2008).
14. J. C. Jung and M. J. Schnitzer, "Multiphoton endoscopy," Opt. Lett. **28**(11), 902–904 (2003).

#142851 - $15.00 USD Received 17 Feb 2011; revised 28 Mar 2011; accepted 29 Mar 2011; published 5 Apr 2011

15. W. Göbel, J. N. Kerr, A. Nimmerjahn, and F. Helmchen, "Miniaturized two-photon microscope based on a flexible coherent fiber bundle and a gradient-index lens objective," Opt. Lett. **29**(21), 2521–2523 (2004).
16. C. J. Engelbrecht, R. S. Johnston, E. J. Seibel, and F. Helmchen, "Ultra-compact fiber-optic two-photon microscope for functional fluorescence imaging in vivo," Opt. Express **16**(8), 5556–5564 (2008).
17. P. Singh, A. Chak, J. E. Willis, A. Rollins, and M. V. Sivak, "In vivo optical coherence tomography imaging of the pancreatic and biliary ductal system," Gastrointest. Endosc. **62**(6), 970–974 (2005).
18. K. König, A. Ehlers, I. Riemann, S. Schenkl, R. Bückle, and M. Kaatz, "Clinical two-photon microendoscopy," Microsc. Res. Tech. **70**(5), 398–402 (2007).
19. M. T. Myaing, D. J. MacDonald, and X. Li, "Fiber-optic scanning two-photon fluorescence endoscope," Opt. Lett. **31**(8), 1076–1078 (2006).
20. X. Li and W. Yu, "Deep tissue microscopic imaging of the kidney with a gradient-index lens system," Opt. Commun. **281**(7), 1833–1840 (2008).
21. M. Mansuripur, *Classical Optics and its Applications*, 2nd ed. (Cambridge University Press, 2009).
22. Y. Zhao, H. Nakamura, and R. J. Gordon, "Development of a versatile two-photon endoscope for biological imaging," Biomed. Opt. Express **1**(4), 1159–1172 (2010).
23. GRINTECH, http://www.grintech.de/grin-lens-systems-for-medical-applications.html
24. R. T. Kester, S. E. Weigum, M. C. Pierce, R. Richards-Kortum, and T. S. Tkaczyk, "Low-cost miniature optics for point-of-care diagnostic instrumentation," Lab Chip (submitted for publication).
25. S. M. Landau, C. Liang, R. T. Kester, T. S. Tkaczyk, and M. R. Descour, "Design and evaluation of an ultra-slim objective for in-vivo deep optical biopsy," Opt. Express **18**(5), 4758–4775 (2010).
26. R. T. Kester, T. S. Tkaczyk, M. R. Descour, T. Christenson, and R. Richards-Kortum, "High numerical aperture microendoscope objective for a fiber confocal reflectance microscope," Opt. Express **15**(5), 2409–2420 (2007).
27. R. T. Kester, T. Christenson, R. R. Kortum, and T. S. Tkaczyk, "Low cost, high performance, self-aligning miniature optical systems," Appl. Opt. **48**(18), 3375–3384 (2009).
28. Y. Wu and X. Li, "Combined influences of chromatic aberration and scattering in depth-resolved two-photon fluorescence endospectroscopy," Biomed. Opt. Express **1**(4), 1234–1243 (2010).
29. S. Bäumer, ed., *Handbook of Plastic Optics* (Wiley-VCH, 2010).
30. M. Bass, ed., *Handbook of Optics*, Volume 2: Devices, Measurements, and Properties (McGraw-Hill, Inc., 1995).
31. M. B. Wabuyele, S. M. Ford, W. Stryjewski, J. Barrow, and S. A. Soper, "Single molecule detection of double-stranded DNA in poly(methylmethacrylate) and polycarbonate microfluidic devices," Electrophoresis **22**(18), 3939–3948 (2001).
32. Y. Konishi, T. Sawaguchi, K. Kubomura, and K. Minami, "High performance cyclo clefin polymer ZEONEX®," Proc. SPIE, 5872 (2005).
33. M. D. Ries, E. Young, L. Al-Marashi, P. Goldstein, A. Hetherington, T. Petrie, and L. Pruitt, "In vivo behavior of acrylic bone cement in total hip arthroplasty," Biomater. **27**(2), 256–261 (2006).
34. M. Petrtyl, Z. Bastl, Z. Krulis, H. Hulejova, M. Polanska, J. Lisal, J. Danesova, and P. Cerny, "Cycloolefin-Copolymer/Polyethylene (COC/PE) Blend Assists with the Creation of New Articular Cartilage," Macromol. Symp. **294**(1), 120–132 (2010).
35. V. Tangpasuthadol, S. M. Pendharkar, R. C. Peterson, and J. Kohn, "Hydrolytic degradation of tyrosine-derived polycarbonates, a class of new biomaterials. Part II: 3-yr study of polymeric devices," Biomaterials **21**(23), 2379–2387 (2000).
36. L. Tabet, C. Bussy, A. Setyan, A. Simon-Deckers, M. J. Rossi, J. Boczkowski, and S. Lanone, "Coating carbon nanotubes with a polystyrene-based polymer protects against pulmonary toxicity," Part. Fibre Toxicol. **8**(3), 3 (2011).
37. M. D. Chidley, K. D. Carlson, R. R. Richards-Kortum, and M. R. Descour, "Design, assembly, and optical bench testing of a high-numerical-aperture miniature injection-molded objective for fiber-optic confocal reflectance microscopy," Appl. Opt. **45**(11), 2545–2554 (2006).
38. K. Obuchi, M. Komatsu, and K. Minami, "High performance optical materials cyclo olefin polymer ZEONEX®," Proc. SPIE, 6671 (2007).
39. J. C. Diels and R. Wolfgang, *Ultrashort Laser Pulse Phenomena* (Elsevier, 2006).
40. R. F. Shi, C. Koeppen, G. Jiang, J. Wang, and A. F. Garito, "Origin of high bandwidth performance of graded-index plastic optical fibers," Appl. Phys. Lett. **71**(25), 3625–3627 (1997).
41. S. N. Kasarova, N. G. Sultanova, C. D. Ivanov, and I. D. Nikolov, "Analysis of the dispersion of optical plastic materials," Opt. Mater. **29**(11), 1481–1490 (2007).
42. W. R. Zipfel, R. M. Williams, and W. W. Webb, "Nonlinear magic: multiphoton microscopy in the biosciences," Nat. Biotechnol. **21**(11), 1369–1377 (2003).
43. K. Sokolov, J. Aaron, B. Hsu, D. Nida, A. Gillenwater, M. Follen, C. MacAulay, K. Adler-Storthz, B. Korgel, M. Descour, R. Pasqualini, W. Arap, W. Lam, and R. Richards-Kortum, "Optical systems for in vivo molecular imaging of cancer," Technol. Cancer Res. Treat. **2**(6), 491–504 (2003).
44. ZEMAX Development Corporation, http://www.zemax.com.
45. A. Tzannes and J. Mooney, "Measurement of the modulation transfer function of infrared cameras," Opt. Eng. **34**(6), 1808–1817 (1995).
46. ISO, ISO 12233:2000 *Photography–Electronic still-picture cameras–Resolution Measurements* (Geneva, Switzerland, 2000).

#142851 - $15.00 USD Received 17 Feb 2011; revised 28 Mar 2011; accepted 29 Mar 2011; published 5 Apr 2011

47. J. Jung, H. Park, J. Park, and H. Kim, "Accuracy of preoperative ultrasound and ultrasound-guided fine needle aspiration cytology for axillary staging in breast cancer," ANZ J. Surg. **80**(4), 271–275 (2010).
48. S. Taneja, A. Jena, K. Kumar, and A. Mehta, "Technical Note: MRI-guided breast biopsy - our preliminary experience," Indian J Radiol Imaging **20**(3), 218–220 (2010).
49. J. E. Kalinyak, K. Schilling, W. A. Berg, D. Narayanan, J. P. Mayberry, R. Rai, E. B. Dupree, D. K. Shusterman, M. A. Gittleman, W. Luo, and C. G. Matthews, "PET-guided breast biopsy," Breast J. **17**(2), 143–151 (2011).

1. Introduction

Multiphoton microscopy imaging modalities, such as two-photon excited fluorescence microscopy (TPM) and second harmonic generation (SHG) imaging, have the potential to provide clinically useful information to advance disease diagnosis [1]. During multiphoton imaging, high temporal energy densities are used to induce non-linear effects in tissue, such as simultaneous absorption of two red photons to excite a molecular UV transition or non-linear scattering.

Two-photon excitation (TPE) occurs when two photons combine to induce an electronic transition equivalent to the sum of the energy of both photons, causing the fluorophore to emit at a wavelength shorter than the excitation wavelength [2,3]. SHG is produced when non-centrosymmetric structures of tissue, such as collagen fibrils, bone matrix, or microtubules [4,5] allow optical field oscillation at twice the frequency of the incident field, thus creating photons at exactly half the wavelength of the incident optical field [4]. The longer excitation wavelengths used by TPM and SHG allow for greater tissue penetration, up to three times deeper than confocal microscopy [6]. Other advantages of multiphoton imaging modalities compared to single photon excitation (SPE) include the inherent sectioning capability of multiphoton imaging, ease of filtering emission light from excitation light compared to SPE fluorescence, and negligible out of focus phototoxicity [6].

The development of miniature two-photon imaging probes began in 2001 with a publication by Helmchen *et al.* [7]. Since that publication, which focused on a "wearable" system for imaging of the brain in freely moving rats, the range of envisioned applications and miniature optical designs has broadened. Miniature multiphoton microscopes are now being developed for use to perform *in vivo* imaging for early cancer detection and cancer research [8–10]. The motivation for miniaturization is to deploy multiphoton imaging deep within intact living tissues or to access organ sites where a conventional microscope cannot reach. This can lead to real-time diagnosis and increased accessibility of research targets, therefore diminishing the need for invasive surgical biopsy or destructive sample preparation. Some applications of miniature multiphoton microscopes include detection of skin cancer [11,12], bladder cancer [1], imaging of gastrointestinal mucosa at the cellular level [13], brain imaging in live animals [14–16], imaging within the pancreatic duct [17], and imaging of the kidney and esophagus in live animals [9].

Most of the miniature microscope designs employ radial gradient index (GRIN) optics to focus light in tissue [9,15,18–20]. However, GRIN lenses were originally developed for coupling light into an optical fiber and not for imaging [21]. Thus, while GRIN lenses can be fabricated in a small size at a low cost, the design degrees of freedom are limited to the diameter, length, and doping profile of the GRIN material and are not enough to fully correct for aberrations which limit image quality and image size. Adding an additional non-GRIN lens on the distal end of the GRIN objective can help to increase the field of view (FOV) and the numerical aperture (NA) and to compensate for aberrations introduced by the GRIN lens. However, this is still not enough to provide good image quality across a reasonable FOV for medical imaging.

An alternative to using GRIN lenses as the focusing optics for endomicroscopes is the proposed ultra-slim objective composed of plastic lenses. The design has a comparable outer diameter (O.D.) to, and larger FOV than, current GRIN objectives [22]. The plastic objective can also maintain consistent performance across the entire FOV, as opposed to commercial GRIN objectives [23].

#142851 - $15.00 USD Received 17 Feb 2011; revised 28 Mar 2011; accepted 29 Mar 2011; published 5 Apr 2011

2. Plastic optics for endomicroscope design

2.1 Ensuring high quality, low cost objectives

Plastic optical systems are inherently mass-producible at low unit cost [24]. As such, they have the potential to become a consumable element of a clinical exam, following the favored "razor/razor-blade" product model. Plastic optics can be fabricated through injection molding or single point diamond turning (SPDT). From a fabrication standpoint, there is no difference between spherical or aspheric surfaces. As a consequence, spherical aberration and other monochromatic aberrations may be corrected with simpler design forms than when only spherical surfaces are available. High-precision element and assembly tolerances can be achieved, in part because optical and mechanical features can be fabricated as part of the same process [25]. Miniature objectives utilizing plastic lenses have been constructed with LIGA springs and spacers which reduce assembly time while maintaining high performance [26,27]. LIGA, a German acronym which translates to x-ray lithography, electroplating, and molding, is a process which allows for the creation of incredibly precise metallic parts, with tolerances on the order of microns. Custom LIGA parts were designed and fabricated to act as the alignment components of the ultra-slim objective; their parameters and use are described further in Section 4.

2.2 Properties of optical plastics with regards to non-linear imaging

Below, the properties of several optical plastics are analyzed to optimize the performance of a non-linear imaging endomicroscope objective. Where applicable, these properties are compared to common optical glasses to provide a reference. When selecting the optical plastic to be used for the creation of the two-photon ultra-slim objective, several material property criteria were considered, including light transmission rate, illumination-induced autofluorescence, induced birefringence due to injection molding, water absorption, heat resistance, and pulse broadening due to group velocity dispersion.

A drawback of using plastic optics is that the available materials offer only a small range of Abbe numbers and indices of refraction compared to the glass catalog. As a result, it is difficult to correct for chromatic aberrations by achromatizing the objective design. Fortunately, a common feature of SHG and TPM is that the excitation light only causes emission from a small voxel of tissue. As a result, the resolution of the endomicroscope objective depends only on the excitation point spread function, so the objective need only be well corrected for the excitation wavelength. However, although achromatization will not improve the resolution of the system, it can improve the collection efficiency of the objective by ensuring that the focal planes of the excitation light and the emission light are conjugate, increasing the throughput of the system [28].

Four common optical plastics were considered. Candidate plastics were Zeonex E48R, which is a cyclo olefin polymer (COP) (Zeon Chemicals L.P., Tokyo, Japan), poly(methyl methacrylate) (PMMA, commonly known as acrylic), polystyrene (PS), and polycarbonate (PC) [29]. Their refractive properties (as well as those for optical glasses BK7 and BaSF10 [30]) are listed in Table 1. E48R and PMMA behave similarly to crown glasses such as BK7. PS and PC, on the other hand, are more like flint glasses, such as BaSF10. With SPDT, the fabrication method selected to create the lenses in the prototype ultra-slim objective, a high-quality diamond tool is used to directly shape the optical surface of the lenses. Because PC quickly degrades the diamond tools when it is used as a substrate for SPDT, it was not prepared for examination at this time.

Table 1. Refractive Properties of Four Optical Polymers and Two Common Glasses [29,30]

Property	E48R	PMMA	PS	PC	BK7	BaSF10
Index of Refraction (nd)	1.53	1.49	1.57	1.57	1.51	1.65
Abbe Number (Vd)	56	57	29	28	64	39

#142851 - $15.00 USD Received 17 Feb 2011; revised 28 Mar 2011; accepted 29 Mar 2011; published 5 Apr 2011

2.2.1 Transmission properties of select optical plastics

The transmission profiles of E48R, PMMA, and PS were measured with a Cary5 spectrophotometer (Agilent Technologies, Santa Clara, CA). As shown in Fig. 1, E48R and PMMA have similar transmission profiles, admitting light from 350 nm through 1100 nm; this range is crucial because the samples will be excited at 780 nm during SHG and at 920 nm during TPM and emit at 390 nm during SHG and between 460 nm and 550 nm during TPM for the selected sample (see Section 5.2).

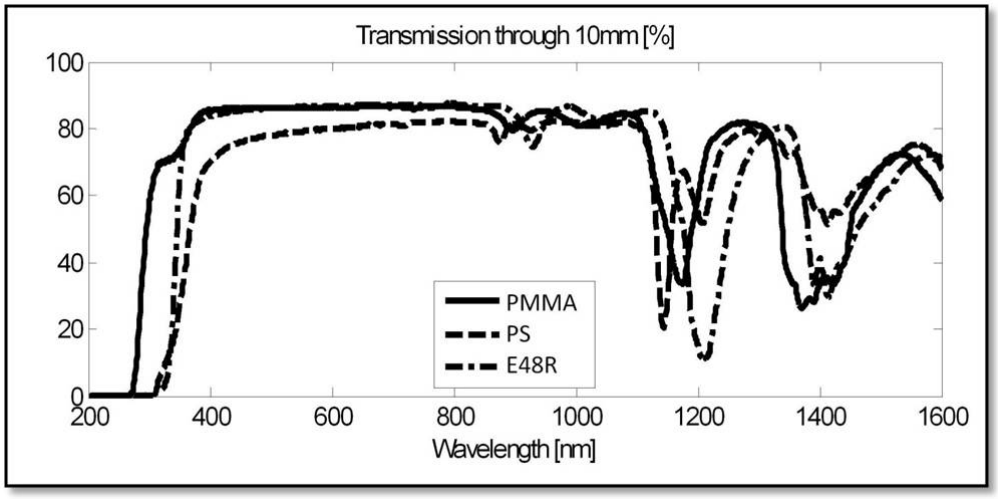

Fig. 1. Wavelength dependent transmission through 10 mm thick optical plastics.

2.2.2 Autofluorescence properties of optical plastics compared to fluorescent solution

A FluoroLog®-3 spectrofluorometer (HORIBA Scientific, Edison, New Jersey, US) was also used to measure the fluorescence spectra of the plastics, as well as a 0.1 microgram per milliliter (μg/mL) solution of fluorescein, a common fluorophore. The results in Fig. 2a show fluorescein has a peak in emission intensity at 490 nm excitation; this excitation wavelength is important because the Argon Ion laser commonly used for biological SPE fluorescence imaging emits at 488 nm. In the excitation bandwidth from 450 nm to 510 nm, the fluorescein solution has an emission intensity that is significantly stronger than the autofluorescence of E48R, PS, and PMMA. Over the specified range, the signal from fluorescein is 10 to 90 times stronger than the signal from E48R, 15 to 100 times stronger than the signal from PS, and 100 to 935 times stronger than the signal from PMMA. As the excitation wavelength increases, the autofluorescence signal generated in E48R, PS, and PMMA decreases. Even at 650 nm, the longest excitation wavelength generated for Fig. 2, E48R, PS, and PMMA had signals that were only 2.9, 3.7, and 1.3 times stronger than the background produced by a water standard, respectively. Other studies have demonstrated the trend of decreasing autofluorescence with increasing wavelength in optical plastics, including PMMA and PC. At 780 nm, both PMMA and PC have low autofluorescence levels which are comparable to glass [31]. Additionally, because the beam never focuses within the lens material, it can be safely assumed that there is no TPE fluorescence effect to generate an autofluorescence signal.

#142851 - $15.00 USD Received 17 Feb 2011; revised 28 Mar 2011; accepted 29 Mar 2011; published 5 Apr 2011

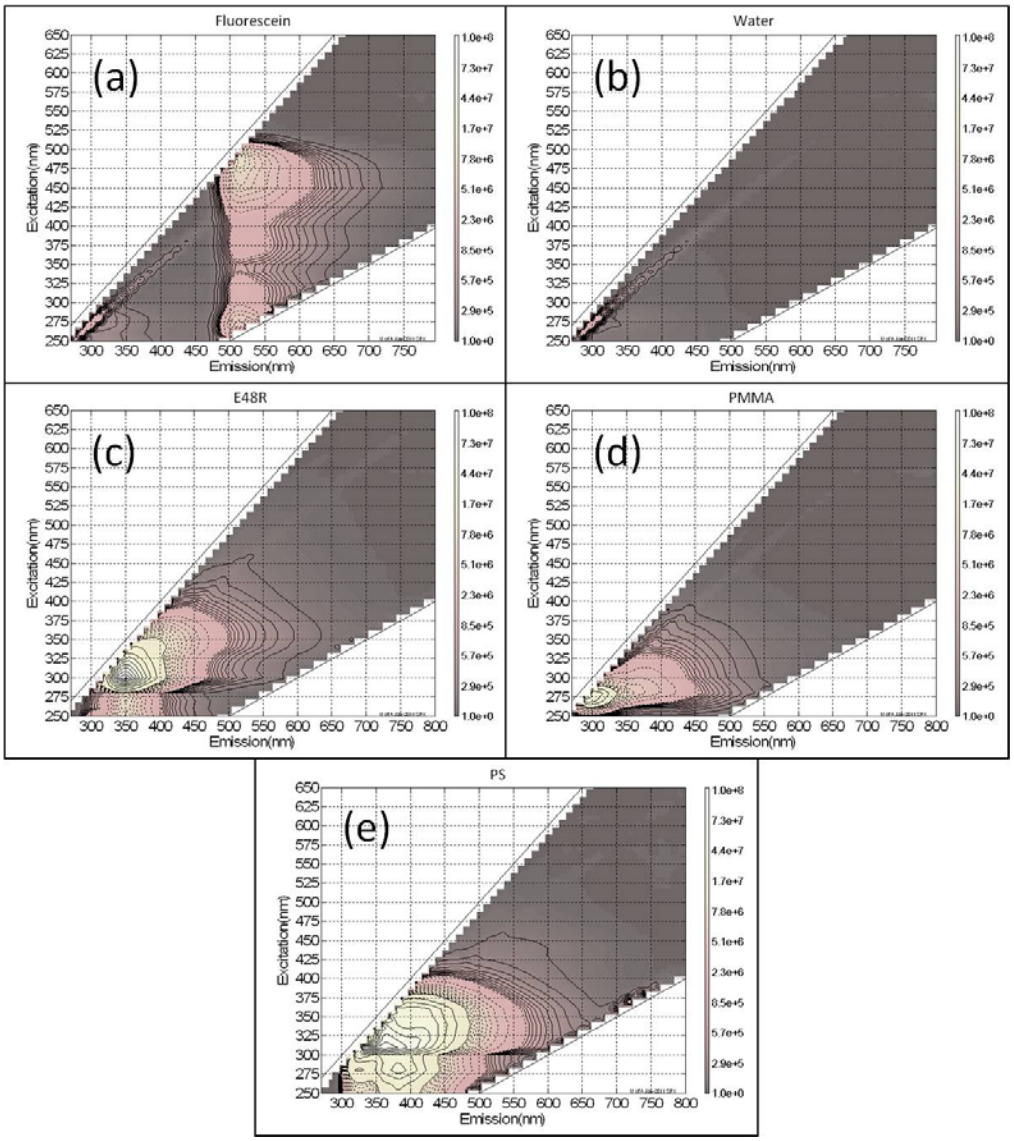

Fig. 2. Autofluorescence data for (a) a 1 μm/mL solution of fluorescein, (b) water, (c) E48R, (d) PMMA, and (e) PS. The X-axis plots the emission wavelength in nanometers, the Y-axis displays the excitation wavelength in nanometers, and color indicates autofluorescence intensity in arbitrary units. Note that the excitation, emission, and intensity scales are the same for all five graphs.

2.2.3 Physical comparison of optical plastics

There are several physical characteristics of optical plastics which can affect the performance of the system, including injection-molding-induced birefringence, water absorption, and heat resistance. These physical properties can negatively affect the quality of the objective if not taken into account during material selection. Both E48R and PMMA have low injection-molding-induced birefringence, while PS and PC are much more susceptible to induced birefringence [32]. It is critical that unintended birefringence be minimized because it has been shown to significantly lower the Strehl ratio of miniature, plastic optical systems [37]. E48R has significantly lower water absorption than PMMA, PS, and PC: <0.01% compared

#142851 - $15.00 USD Received 17 Feb 2011; revised 28 Mar 2011; accepted 29 Mar 2011; published 5 Apr 2011

to approximately 0.3%, 0.03-0.1%, and 0.2%, respectively [29,38]. This is particularly important for the first lens in the system, which is in direct contact with an aqueous solution during imaging. Less water absorption reduces the amount of deformation undergone by the lens' surface, which in turn reduces the degradation of the optical performance. Water absorption also causes a change in the index of refraction of the optical material, which can further reduce performance of the objective. E48R has higher heat resistance compared to PMMA, which further increases its ability to maintain high quality optical performance [32].

Because the lenses are intended to be used in an *in vivo* setting, it is important to determine the potential toxicity of the plastics. PMMA, COPs (such as E48R), and PC have both been shown to be biocompatible as bone cement, which requires them to be implanted for far longer than they would be used for imaging [33–35]. PS has actually been used to prevent cytotoxicity *in vivo* [36]. Clearly, any of the optical plastics have sufficient biocompatibility to form the lenses of an *in vivo* optical system.

2.2.4 Pulse broadening due to group velocity dispersion in select optical plastics and glasses

As with conventional TPM using glass optics, pulse broadening due to group velocity dispersion (GVD) is a concern [39]. However, the literature regarding group velocity dispersion in plastic is very sparse [40]. As the pulse width of the excitation light increases, a higher intensity pulse is necessary to maintain the generation of signal, which risks damage to both the tissue and the plastic lenses (see the optical design in Section 4). The group delay dispersion (GDD) for the material was calculated from the GVD,

$$\mathrm{GDD} = \mathrm{GVD} \times L, \tag{1}$$

where L is the length of material the light propagates through. GDD represents the amount of dispersion, and thus pulse broadening, through a particular system. GVD can be calculated using the equation from [39]

$$\mathrm{GVD} = \frac{\lambda^3}{2\pi c^2}\frac{\mathrm{d}^2 n}{\mathrm{d}\lambda^2}, \tag{2}$$

where λ is the wavelength of light at the source and c is the speed of light in a vacuum. Equation (2), in turn, requires the second derivative of the index of refraction to be calculated in terms of wavelength. For this, we start with the equation for the index of refraction, n, using the modified Cauchy equation and accompanying dispersion coefficients provided in [41]

$$n = \left(A_1 + A_2\lambda^2 + \frac{A_3}{\lambda^2} + \frac{A_4}{\lambda^4} + \frac{A_5}{\lambda^6} + \frac{A_6}{\lambda^8}\right)^{1/2}. \tag{3}$$

Taking the second derivative with respect to λ leads to

$$\frac{\mathrm{d}^2 n}{\mathrm{d}\lambda^2} = \frac{1}{2}\left\{\begin{array}{l}\dfrac{-1}{2}\left[\left(A_1 + A_2\lambda^2 + \dfrac{A_3}{\lambda^2} + \dfrac{A_4}{\lambda^4} + \dfrac{A_5}{\lambda^6} + \dfrac{A_6}{\lambda^8}\right)^{-3/2}\left(2A_2\lambda - 2\dfrac{A_3}{\lambda^3} - 4\dfrac{A_4}{\lambda^5} - 6\dfrac{A_5}{\lambda^7} - 8\dfrac{A_6}{\lambda^9}\right)^2\right] \\ +\left(A_1 + A_2\lambda^2 + \dfrac{A_3}{\lambda^2} + \dfrac{A_4}{\lambda^4} + \dfrac{A_5}{\lambda^6} + \dfrac{A_6}{\lambda^8}\right)^{-1/2}\left(2A_2 + 6\dfrac{A_3}{\lambda^4} + 20\dfrac{A_4}{\lambda^6} + 42\dfrac{A_5}{\lambda^8} + 72\dfrac{A_6}{\lambda^{10}}\right)\end{array}\right\}. \tag{4}$$

which can be used to solve for GVD and, in turn, GDD.

Table 2 contains the GDD and GVD data for E48R, PMMA, PS, PC, BK7, and BaSF10. At 780 nm, BK7 has the lowest GVD (and thus creates the smallest amount of pulse broadening). PMMA, E48R, and BaSF10 all have similar dispersion, which is lower than that for PS and PC. All the materials have lower dispersion at 920 nm than at 780 nm. Note that

#142851 - $15.00 USD Received 17 Feb 2011; revised 28 Mar 2011; accepted 29 Mar 2011; published 5 Apr 2011

for PMMA and E48R, the GVD is negative at 920 nm; this will create pulse broadening of the same magnitude but in the opposite direction of the pulse as would occur if the GVD was positive [39]. It also means that PMMA or E48R could be combined with PC or PS to achieve near zero net GDD at this wavelength.

The GDD data can be used to calculate the change in pulse width caused by propagation through the material with the equation [39]

$$\Delta t_{out} = \frac{\sqrt{\Delta t^4 + 16(\ln 2)^2 (\mathrm{GDD})^2}}{\Delta t}, \tag{5}$$

where Δt is the pulse width of light entering the objective and Δt_{out} is the pulse width upon exiting the material. Table 2 shows that, for a 130 fs pulse traveling through 7 mm of material (an amount approximately equal to the length of the ultra-slim objective), the pulse width has broadened by 2.9 fs or less, depending on the material. The pulse width of 130 fs is the duration of the pulses used to perform the initial SHG and TPM imaging described in Section 5. The wavelengths of 780 nm and 920 nm are used for SHG and TPM in the imaging experiments described in Section 5.1 and Section 5.2, respectively. This demonstrates that the objective does not significantly contribute to pulse broadening for the given experimental setup. However, for shorter pulses, GVD becomes a significant factor with regards to pulse broadening. Table 2 shows that when the initial pulse width is reduced to 10 fs, the change in pulse width due to GVD increases by anywhere from a factor of two to more than an order of magnitude. It should be noted that glass suffers from similar pulse broadening at this pulse width and wavelength.

Table 2. Group Velocity Dispersion Data for Six Optical Materials

Property	Δt	PMMA	E48R	PS	PC	BK7	BaSF10
GVD_{780nm} (fs^2mm^{-1})		104.1	104.9	173.8	183.8	55.5	106.7
GDD_{780nm} (fs^2)[a]		0.73	0.73	1.22	1.29	0.39	0.75
GVD_{920nm} (fs^2mm^{-1})		–31.4	–11.5	57.3	39.7	42.2	83.1
GDD_{920nm} (fs^2)[a]		–0.22	–0.08	0.40	0.28	0.30	0.58
$\Delta t_{out,\ 780nm}$ (fs)	130	130.9	130.9	132.6	132.9	130.6	131.0
$\Delta t_{out,\ 780nm}$ (fs)	10	202.4	203.8	337.5	356.9	108.3	207.2
$\Delta t_{out,\ 920nm}$ (fs)	130	130.1	130.0	130.3	130.1	130.2	130.6
$\Delta t_{out,\ 920nm}$ (fs)	10	61.7	24.5	111.7	77.7	82.6	161.7

[a]GDD is calculated for the pulse travelling through 7 mm of material.

2.2.5 Justification of selected optical plastic

Zeonex E48R was selected as the optical material for the ultra-slim, non-linear endomicroscope objective. It has similar properties to PMMA in terms of index of refraction, Abbe number, light transmission, induced birefringence, and pulse broadening. E48R has superior heat resistance and reduced water absorption. PMMA has better autofluorescence characteristics at single-photon excitation wavelengths compared to E48R; however, our objective is designed for use in the near-IR, where autofluorescence of plastics is negligible. More important is the ability to resist water absorption, as the objective is designed for *in vivo* use and thus will experience water immersion in object space.

3. Overview of the ultra-slim endomicroscope objective

To demonstrate that plastic optics can be used for two-photon microscopy imaging, we have designed, constructed, and tested a prototype ultra-slim endomicroscope objective to collect the first SHG and TPM images with an all plastic optical system. Compared to a previous ultra-slim objective design [25], this objective has been modified for use with multiphoton imaging and to improve tolerancing of the design based on assembly procedures. The design

#142851 - $15.00 USD Received 17 Feb 2011; revised 28 Mar 2011; accepted 29 Mar 2011; published 5 Apr 2011

has been incorporated into a 1.27 mm O.D. hypodermic tube. A summary of the design specifications is given in Table 3.

Table 3. Design specifications of Two-Photon Needle Objective

Object Space NA[a]	0.4
Image Space NA	0.125
Field of View (FOV)	250 μm
Clear Aperture	0.8 mm
Magnification	–3.2
Working Distance[a]	200 μm
Wavelength	900 nm
Telecentricity	Object Space

[a]Object space is designed for water immersion.

The object space NA of 0.4 provides, for single photon imaging, a theoretical transverse resolution of 1.19 μm for an illumination wavelength of 780 nm and a resolution of 1.40 μm for an illumination wavelength of 920 nm. The corresponding theoretical depth of field is 6.48 μm at 780 nm and 7.65 μm at 920 nm in tissue. During SHG and TMP, however, the lateral resolution and depth of field may be significantly smaller due to non-linear effects [42]. The FOV of 250 μm was selected to ensure that a sufficient number of epithelial cells, which have a diameter of approximately 10 μm, will be seen within a single image. The ability to image a large number of epithelial cells is important because early diagnosis of cancer typically takes place by examining the tissue for suspicious lesions; in order to detect these lesions and differentiate them from healthy tissue, clinicians desire a large FOV with subcellular resolution [43]. Object space telecentricity ensures that the image magnification is independent of the object's position in, or distance from, the focal plane.

4. Optical design of needle lens

ZEMAX [44] was used to develop a lens system which meets the specified criteria. It utilizes three custom plastic lenses which incorporate aspheric surfaces to aid in the correction of aberrations. The design is illustrated in Fig. 3. The object surface has a curvature (radius of 0.8 mm across the 250 μm FOV), which helps to correct for aberrations in the system. This is allowable because the objective is intended to image three-dimensional tissues and the sag introduced by the curved image plane is less than 10 μm, which is the approximate thickness of a single layer of epithelial cells. The prescription data for the design is listed in Table 4. The lens material is Zeonex E48R which can be shaped through SPDT and injection molding to produce high quality optical components. For prototyping, SPDT was used to create the lenses, as it allows a small numbers of parts to be made and can easily accommodate changes in design. Ultimately, injection molding will be used to fabricate larger quantities of lenses.

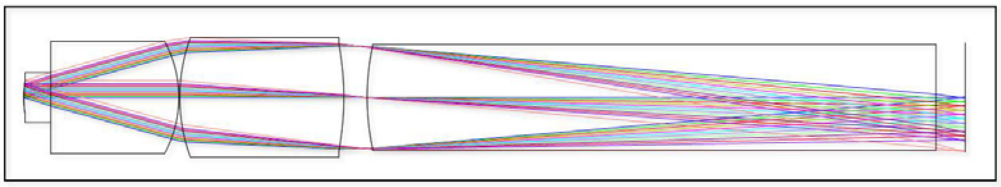

Fig. 3. Needle objective optimized for two-photon imaging. Total length = 6.98 mm

The objective is assembled within 18 gauge hypodermic tubing (Small Parts, Inc, Miramar, Florida, USA), which was measured to have an O.D. of 1.27 mm and an inner diameter of 1.072 mm. The assembly procedure is described in [27]. It has been simplified by using a single type of LIGA part; each identical part acts as both a spring and a spacer (Fig. 4). The O.D. of the first lens is precisely controlled so that it can be press-fit into the hypodermic tubing. The lens is pushed into place using a 0.0422" (1.072 mm) precision gage pin (Deltronic, Santa Ana, California, USA) so that 100-200 μm of lens material extends

#142851 - $15.00 USD Received 17 Feb 2011; revised 28 Mar 2011; accepted 29 Mar 2011; published 5 Apr 2011

beyond the edge of the tube. Two 85 μm thick springs, each having an O.D. of 1122 μm when the arms are fully extended, are inserted between the first and second lenses, then pressed into place using the gage pin. The springs serve several purposes. They precisely define the spacing between lenses to within 10 μm in order to create an air gap with the designed thickness [27]. They force the lenses to center within the tube to a tolerance of less than 10 μm, with less than 3 mrad of tilt [27]. These values are within the tolerances budgeted for the design. The springs also limit the clear aperture of the lenses to 0.8 mm. Three more springs are placed between lens two and lens three. A final spring is placed after the third lens to hold the components in place. Norland optical adhesive (NOA) 61 (Norland Products, Inc., Cranbury, New Jersey, US) is used to seal the object side of the ultra-slim objective for water immersion.

Table 4. Lens Prescription Data

Surface	Comment	Radius	Thickness	Material	Conic
Object	Tissue	0.8000	0.200	SEAWATER	0.0000
1	Lens 1	Infinity	0.950	E48R	0.0000
2		–0.8613	0.007		0.0000
3	Lens 2	1.2744	1.217	E48R	0.0000
4		–1.9356	0.173		–12.1922
STOP	Lens 3	1.7992	4.219	E48R	–0.4300
5		Infinity	0.217		0.0000
Image		Infinity	0.000		0.0000

The imaging performance of the ultra-slim objective was evaluated using a 1951 USAF resolution target (NT36-275, Edmund Optics Inc., Barrington, NJ, US) by estimating the Strehl ratio (SR). The SR, which is the ratio of peak irradiance in the Airy disk from the experimental system to the peak irradiance in the Airy disk of a diffraction-limited system, can be estimated by finding the ratio of the area under the MTF of the measured system to the that of the theoretical diffraction-limited system. For the ultra-slim objective, the SR was estimated by imaging a black and white edge on the resolution target with 800 nm trans-illumination and performing the slanted edge MTF technique [45,46] near the center of the FOV. This technique estimates the MTF of the system by measuring the contrast between the black and white regions at the detector. This data can be used to find the MTF of the experimental system, and from that to estimate the SR. The objective used to perform the study in Section 5 had a SR of 0.85; a value above 0.8 is generally considered diffraction limited performance. The measured magnification at the image plane was 3.19 for the best conjugate plane.

5. Multiphoton microscopy imaging results through the all-plastic objective

A benchtop microscope system (TrimScope, LaVision BioTec, Bielefeld, Germany) was used to perform SHG and TPM with the ultra-slim objective. The samples were excited using a Chameleon Ultra 2 Ti:Sapphire laser (Coherent Inc, Santa Clara, California, US). The tuning range of the laser is 680 nm to 1080 nm. The pulse width at the source is 130 fs and has a repetition rate of 80 MHz. The average power at the input of the ultra-slim objective was 5 mW for both SHG and TPE. The images were recorded through non-descanning reverse detection. The ultra-slim objective imaged the sample and a commercial objective (UPlanFL 4 × /0.13, Olympus Corp., Tokyo, Japan) on the benchtop system relayed the intermediate image plane to a photomultiplier tube (PMT) detector in non-descanned configuration. A diagram of the experimental setup is illustrated in Fig. 5. Two samples, rat-tail collagen fibers and *Convallaria*, commonly known as lily of the valley, were imaged to test the capabilities of the plastic objective to image via SHG and TPM, respectively.

#142851 - $15.00 USD Received 17 Feb 2011; revised 28 Mar 2011; accepted 29 Mar 2011; published 5 Apr 2011

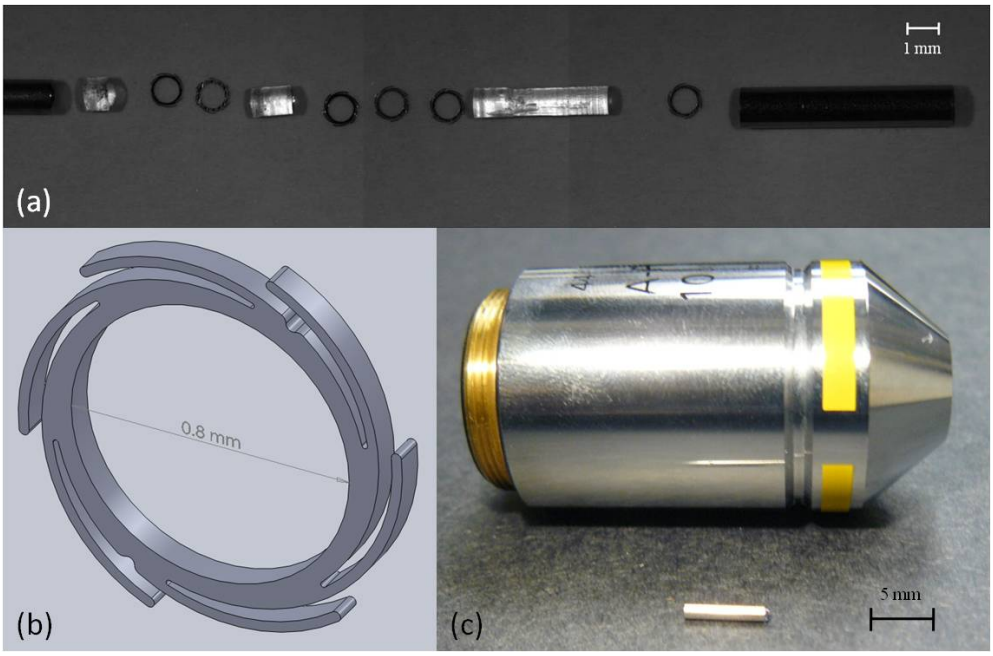

Fig. 4. (a) Exploded view of an ultra-slim objective. The left rod is a precision gage pin used to insert the parts into the hypodermic tubing. The clear plastic pieces are the custom lenses. The circular rings are LIGA springs which act as alignment devices and apertures. On the right is the hypodermic tubing used to house the objective. (b) SolidWorks model of the LIGA springs. (c) The ultra-slim objective next to a conventional microscope objective for size comparison.

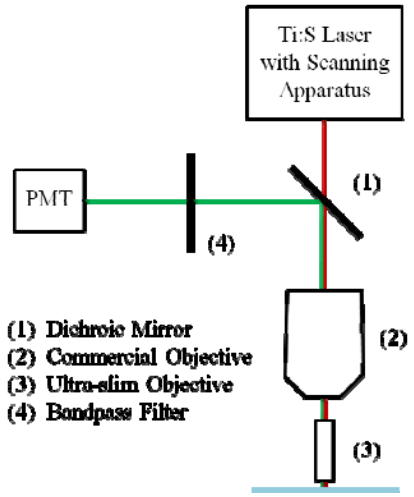

Fig. 5. Schematic of the non-linear imaging setup used to test the ultra-slim objective. The light was generated by a laser and scanned through a dichroic mirror (1) and into a commercial, NA 0.13 objective (2). The excitation light was focused by the commercial objective onto the back image plane of the ultra-slim objective (3), which transferred the light onto the sample. The emission light was collected by the ultra-slim objective, relayed by the commercial objective, and reflected by the dichroic mirror before passing through an emission filter (4) and being detected by a PMT.

5.1 Imaging of Second Harmonic Generation (SHG) in rat-tail collagen fibers

The rat-tail collagen fiber sample was extracted from the rat-tail, fixed, and attached to a glass slide. The specimen was illuminated at 780 nm and observed through a bandpass filter

#142851 - $15.00 USD Received 17 Feb 2011; revised 28 Mar 2011; accepted 29 Mar 2011; published 5 Apr 2011

centered at 377 nm with a 50 nm bandwidth (FF01-377/50, Semrock Inc, Rochester, New York, US) after reflecting off a 405 nm dichroic mirror (Di01-R405-25x36, Chroma Technology Corp, Bellows Falls, Vermont, US). Figure 6a shows a 995x995 pixel image of a single slice of rat-tail collagen obtained with SHG. Notice the striation of the collagen fibers.

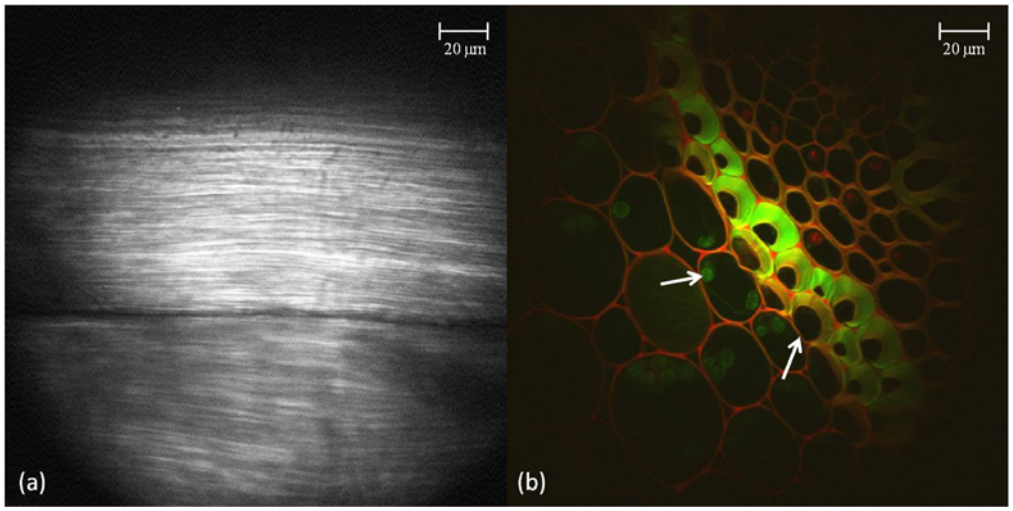

Fig. 6. (a) An enlarged view of a rat tail tendon optical section taken via SHG with the ultra-slim objective in series with the benchtop system. (b) A false-color image shows *Convallaria* cells imaged via TPM at two different wavelengths, also with the ultra-slim objective. The left arrow points to a green nucleus and while the right arrow points to a red cell membrane.

5.2 Imaging of two-photon excited fluorescence in *Convallaria*

A *Convallaria* rhizome cross-section specimen was used to test the capability of the plastic objective to image TPE signal (Johannes Lieder GmbH & Co. KG, Ludwigsburg, Germany). The *Convallaria* specimen was stained with acridine orange, mounted beneath a glass coverslip, and imaged through a layer of water between the glass and the ultra-slim objective. The specimen was illuminated at 920 nm and observed through a 680-nm shortpass filter in series with a standard GFP emitter bandpass filter.

Figure 6b shows a 995x995 pixel, false-color image of the *Convallaria* sample via the ultra-slim endomicroscope objective. Green light corresponds to a signal which has been filtered through a bandpass filter centered at 460 nm with a bandwidth of 80 nm (FF02-460/80, Semrock) and detected by a Galium Arsenide PMT (H7422A-40, Hamamatsu), while red light corresponds to a signal which has passed through a 505 nm dichroic mirror (505DCXR, Chroma) before being filtered by a bandpass filter centered at 550 nm with a bandwidth of 88 nm (FF01-550/88, Semrock) and detected by a Bialkali PMT (H6780-01, Hamamatsu). Notice the ability of the objective to resolve subcellular features such as nuclei and cell membranes.

6. Conclusions

The ability to perform TPM and SHG imaging has been demonstrated using a 1.27 mm O.D., NA = 0.4, FOV = 250 μm plastic, multi-lens, all-refractive objective. To the best of our knowledge, this is the smallest integrated microscope objective of this type ever made. The ultra-slim objective demonstrates diffraction-limited performance and was designed as a prototype to be used for non-linear endoscopic imaging. It can be used to acquire high resolution, high contrast *in vivo* images with no need for exogenous contrast agents to provide morphological information for diagnostic applications, such as early cancer detection. These miniature microscope objectives have the potential to help in localization of suspicious

#142851 - $15.00 USD Received 17 Feb 2011; revised 28 Mar 2011; accepted 29 Mar 2011; published 5 Apr 2011

lesions, to pinpoint biopsy sites, and to reduce the overall number of invasive biopsies performed. The ultra-slim objective is envisioned as being used to probe tissue that has already been deemed abnormal by large FOV, low resolution imaging such as traditional endoscopy; the ultra-slim objective is narrow enough to fit through a standard port on an endoscope. Ultrasound imaging [47], MRI [48], and positron emission mammography [49] are other large FOV, low resolution imaging techniques which have been used to guide conventional biopsy needles to suspicious tissue; it is feasible to also perform a similar procedure with the ultra-slim objective.

In the future, the NA of the objective can be increased to improve excitation and collection efficiency; this may be accomplished by substituting the first plastic lens in the system for a high-power glass lens as done by Kester *et al.* [27]. It may also be advantageous to increase the FOV so that clinicians may assess a larger region of interest.

Using all-refractive, plastic optics in endomicroscope objectives enables the easy use of aspheric surfaces which simplifies the design and allows the number of elements to be reduced. The examined optical plastics had high rates of transmission from 400 nm to 1100 nm, low GVD for the selected illumination wavelengths, and low autofluorescence for near-IR illumination, making them suitable for non-linear imaging. PMMA and Zeonex E48R also have low injection-molding induced birefringence, while E48R has higher heat-resistance and lower water absorption than PMMA. These factors make the presented design a good candidate for the fabrication of optical components via injection molding. If used with zero-alignment techniques, such as utilizing high-precision, self-centering mounts, these integrated miniature objectives can be built as high-performance, disposable optical needles used in a variety of *in vivo* applications.

Acknowledgments

The project is supported in part by an IBB Medical Innovation Award supported by the Sid W. Richardson Foundation to T. Tkaczyk and by grants R01 EB007594, R01 CA124319, S10 RR023737.

#142851 - $15.00 USD Received 17 Feb 2011; revised 28 Mar 2011; accepted 29 Mar 2011; published 5 Apr 2011